CHEMISTRY
A EUROPEAN JOURNAL

DOI: 10.1002/chem.201002110

Synthesis, Crystal Structures and Magnetic Properties of $M^{II}Cu^{II}$ Chains (M = Mn and Co) with Sterically Hindered Alkyl-Substituted Phenyloxamate Bridging Ligands**

Jesús Ferrando-Soria,[a] Emilio Pardo,*[a] Rafael Ruiz-García,[a, b] Joan Cano,[a, b] Francisco Lloret,*[a] Miguel Julve,[a] Yves Journaux,*[c] Jorge Pasán,[d] and Catalina Ruiz-Pérez[d]

Abstract: A series of neutral oxamato-bridged heterobimetallic chains of general formula $[MCu(L^x)_2(S)_2]\cdot p\,S\cdot q\,H_2O$ [$p = 0$–1, $q = 0$–2.5; $L^1 = N$-2,6-dimethylphenyloxamate, S = DMF with M = Mn (**1a**) and Co (**1b**); $L^2 = N$-2,6-diethylphenyloxamate, S = DMF with M = Mn (**2a**) and Co (**2b**) or S = DMSO with M = Mn (**2c**) and Co (**2d**); $L^3 = N$-2,6-diisopropylphenyloxamate, S = DMF with M = Mn (**3a**) and Co (**3b**) or S = DMSO with M = Mn (**3c**) and Co (**3d**)] were prepared by treating the corresponding anionic oxamatocopper(II) complexes $[Cu(L^x)_2]^{2-}$ ($x = 1$–3) with M^{2+} cations (M = Mn and Co) in DMF or DMSO as the solvent. The single-crystal X-ray structures of **2a** and **3a** reveal the occurrence of well-isolated, zigzag, oxamato-bridged manganese(II)–copper(II) chains. The intrachain Cu···Mn distances across the oxamato bridge are 5.3761(7) and 5.4002(17) Å for **2a** and **3a**, respectively, whereas the shortest interchain Mn···Mn distances are 9.4475(16) and 8.1649(14) Å for **2a** and **3a**, respectively. All of these $M^{II}Cu^{II}$ chains (M = Mn and Co) exhibit 1D ferrimagnetic behaviour with moderately strong intrachain antiferromagnetic coupling between the square-planar Cu^{II} and octahedral high-spin M^{II} ions across the oxamato bridge [$-J = 31.4$–35.2 and 33.4–44.8 cm^{-1}, respectively; $\mathbf{H} = \Sigma_i - J\mathbf{S}_{M,i}(\mathbf{S}_{Cu,i} + \mathbf{S}_{Cu,i-1})$]. Only the $Co^{II}Cu^{II}$ chains show slow magnetic relaxation effects characteristic of single-chain magnets (SCMs). Analysis of the magnetic relaxation dynamics of **3d** shows a thermally activated mechanism (Arrhenius law dependence) with values of the pre-exponential factor ($\tau_0 = 2.6 \times 10^{-9}$ s) and activation energy ($E_a = 7.7$ cm^{-1}) that are typical of SCMs. In contrast, two relaxation regimes are observed for **2d** in different temperature regions ($\tau_0 = 3.2 \times 10^{-10}$ s and $E_a = 24.7$ cm^{-1} for $T < 4.5$ K and $\tau_0 = 3.2 \times 10^{-14}$ s and $E_a = 37.5$ cm^{-1} for $T > 4.5$ K).

Keywords: chain structures · cobalt · copper · magnetic properties · manganese

[a] J. Ferrando-Soria, Dr. E. Pardo, Dr. R. Ruiz-García, Dr. J. Cano, Prof. Dr. F. Lloret, Prof. Dr. M. Julve
Departament de Química Inorgànica/Instituto de Ciencia Molecular (ICMol)
Universitat de València, Paterna, Valencia, 46980 (Spain)
Fax: (+34) 963544322
E-mail: emilio.pardo@uv.es
francisco.lloret@uv.es

[b] Dr. R. Ruiz-García, Dr. J. Cano
Fundació General de la Universitat de València (FGUV)
Universitat de València, Valencia, 46002 (Spain)

[c] Dr. Y. Journaux
Institut Parisien de Chimie Moléculaire, UMR CNRS 7071
UPMC-Univ. Paris 06, Paris, 75005 (France)
Fax: (+33) 144273841
E-mail: yves.journaux@upmc.fr

[d] Dr. J. Pasán, Prof. Dr. C. Ruiz-Pérez
Laboratorio de Rayos X y Materiales Moleculares
Departamento de Física Fundamental II
Facultad de Física, Universidad de la Laguna
La Laguna, Tenerife, 38201 (Spain)

[**] Ligand Design for Heterobimetallic Single-Chain Magnets, Part 2; for Part 1, see: E. Pardo, R. Ruiz-García, F. Lloret, J. Faus, M. Julve, Y. Journaux, M. A. Novak, F. S. Delgado, C. Ruiz-Pérez, *Chem. Eur. J.* **2007**, *13*, 2054.

Supporting information for this article is available on the WWW under http://dx.doi.org/10.1002/chem201002110.

Introduction

The observation of slow magnetic relaxation effects below a blocking temperature (T_B) in molecule-based chain compounds a decade ago,[1] providing experimental confirmation of Glaubers' prediction,[2] opened exciting perspectives for storing information in low-dimensional molecular magnetic materials.[3] This novel class of magnetic chain compounds has been referred to as single-chain magnets (SCMs) by analogy to the so-called single-molecule magnets (SMMs). SMMs have a high-spin (S) ground state with an important Ising-type magnetic anisotropy (D) that results in a large activation energy (E_a) for magnetisation reversal, given by $E_a = |D|S^2$.[4] In the case of SCMs, the activation energy also depends upon the intrachain magnetic coupling (J) according to the expression $E_a = (4|J| + |D|)S^2$.[5] In recent years, many groups have focused their efforts on the search for SCMs because of the possibility of increasing the value of T_B by modifying the intrachain interactions and thus opening the way to future applications in nanoscience and nanotechnology.

Since the discovery of the first SCM, a cobalt(II) nitronyl nitroxide radical chain with the formula $[Co(hfac)_2(NITPhOMe)]$ (hfac = hexafluoroacetylacetonate, NITPhOMe = 4′-methoxyphenyl-4,4,5,5-tetramethylimidazoline-1-oxyl-3-oxide), by Gatteschi et al.,[1] some other examples have been reported.[6–11] Recent reviews by Clérac et al.[5a,b] and Gao et al.[5c] classified SCMs by taking into account the synthetic strategies and preparative routes towards the chain compound, the role of the bridging ligand and the nature of the magnetic coupling, either ferro- or antiferromagnetic, between neighbouring ions along the chain. Some fundamental questions related to the understanding of the relaxation mechanism in these 1D systems remain open and, therefore, further experimental work is required to obtain new examples of SCMs. The conditions to be fulfilled for the observation of this magnetic behaviour could be summarised as the existence of an easy axis of magnetization and a high ratio of intra- to interchain magnetic coupling ($|J/j| > 10^4$). Accordingly, synthetic strategies to build new SCMs have focussed on the search for the perfect system combining highly anisotropic transition-metal (Co^{II}, Fe^{II} and Mn^{III}) and/or lanthanide ions (Dy^{III}, Tb^{III} and Ho^{III}) with bridging ligands to give strong ferro- or antiferromagnetic interactions between the metal centres while maintaining good isolation between the chains.

Previously, we presented a rational strategy to obtain SCMs based on the use of sterically hindered, dianionic oxamatocopper(II) complexes as bis-bidentate ligands (metalloligands) toward solvated divalent transition-metal cations like manganese(II) or cobalt(II) in either dimethyl sulfoxide or water as solvent (Scheme 1).[11b] The resulting family of $M^{II}Cu^{II}$ chains (M = Mn and Co) with 2-, 2,6- and 2,4,6-polymethyl-substituted phenyloxamate bridging ligands behave as ferrimagnetic chains with a moderately large intrachain antiferromagnetic coupling between Cu^{II} and M^{II} ions. The $Mn^{II}Cu^{II}$ chains show evidence of neither slow magnetic relaxation effects nor 3D long-range ferromagnetic ordering, as expected from the magnetically isotropic character of the octahedral high-spin Mn^{II} ion with a $^6A_1$ single-ion ground state ($D \approx 0$) and the very good isolation of the chains ($j \approx 0$). In contrast, some of the $Co^{II}Cu^{II}$ chains show slow magnetic relaxation effects at low temperatures typical of SCMs because of the magnetically anisotropic character of the octahedral high-spin Co^{II} ion with an orbitally degenerate $^4T_1$ single-ion ground state. Moreover, when the number of methyl substituents along the series of $Co^{II}Cu^{II}$ chains is increased from one to three, the T_B values increase in accordance with the steric hindrance of the aryl-substituted oxamate ligand. This observation is likely related to the greater separation between chains, and hence to the decrease in interchain interactions. In addition, the nature of the solvent is another factor that significantly influences the SCM behaviour. Thus, higher T_B values are observed for the $Co^{II}Cu^{II}$ chains with DMSO compared to those with aqua ligands and/or water of crystallisation, probably due to better isolation of the chains because of the larger size of the former. Although the influence of the interchain interactions on the slow relaxation dynamics of SCMs has been predicted theoretically,[12] experimental studies are still scarce[13] compared to the related SMMs.[14–16]

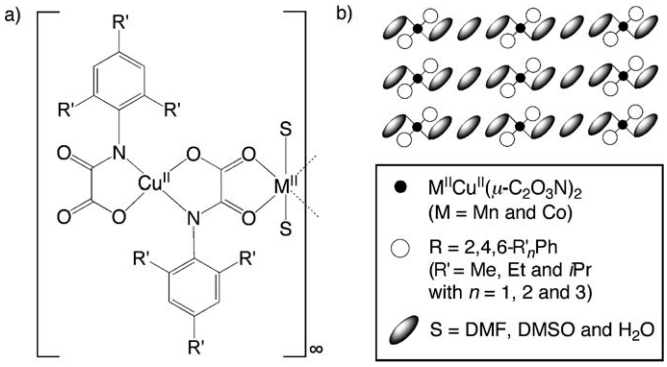

Scheme 1. Ligand design strategy toward oxamato-bridged heterobimetallic SCMs of general formula $[Cu^{II}(\mu\text{-}C_2O_3NR)_2M^{II}(S)_2]_\infty$ (R = 2,4,6-R′$_n$Ph with R′ = Me, Et and *i*Pr and n = 1–3; M = Mn and Co; S = DMF, DMSO and H_2O).

As an extension of this work, herein we report the synthesis and structural and magnetic characterisation of a new series of heterobimetallic chains of general formula $[M^{II}Cu^{II}(L^x)_2(S)_2]\cdot p\,S\cdot q\,H_2O$ (M = Mn or Co; S = DMF or DMSO; x = 1–3), prepared from the corresponding mononuclear copper(II) complexes, $[Cu^{II}(L^x)_2]^{2-}$ (L^1 = *N*-2,6-dimethylphenyloxamate, L^2 = *N*-2,6-diethylphenyloxamate, and L^3 = *N*-2,6-diisopropylphenyloxamate; Scheme 1a). A comparison of the static and dynamic magnetic properties in this family of oxamato-bridged $M^{II}Cu^{II}$ chains with sterically hindered, 2,6-dialkyl-substituted, phenyloxamate bridging ligands is presented. The influence of the intra- and interchain magnetic interactions and the local magnetic anisotropy on the SCM behaviour was analysed by varying the size of the alkyl substituents of the aromatic ring in the copper(II) precursor (R′ = Me, Et, *i*Pr) and the nature of the coor-

dinated solvent molecules and solvent molecules of crystallisation (S = DMF and DMSO; Scheme 1b).

Results and Discussion

Synthesis and general physical characterization: The neutral oxamato-bridged $M^{II}Cu^{II}$ chains (M = Mn and Co) were synthesised in three successive steps (Scheme 2). First, 2,6-di-

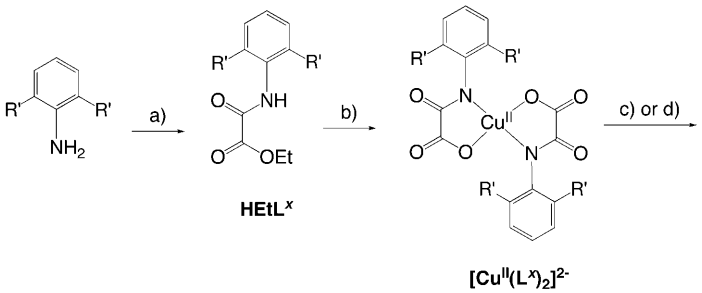

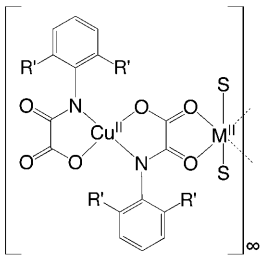

	M	L^x	R'	S	p	q
1a	Mn	L^1	Me	DMF	0	0
2a	Mn	L^2	Et	DMF	0	0
3a	Mn	L^3	*i*Pr	DMF	1	1
1b	Co	L^1	Me	DMF	0	0
2b	Co	L^2	Et	DMF	0	0
3b	Co	L^3	*i*Pr	DMF	0	2.5
2c	Mn	L^2	Et	DMSO	0	0
3c	Mn	L^3	*i*Pr	DMSO	0.5	2.5
2d	Co	L^2	Et	DMSO	1	2
3d	Co	L^3	*i*Pr	DMSO	0.5	0

Scheme 2. Synthetic pathway to the oxamato-bridged heterobimetallic chain compounds: a) C_2O_2ClOEt, THF, 70 °C; b) NaOH/$Cu(NO_3)_2$, H_2O, RT; c) $M(NO_3)_2$ (M = Co, Mn), DMF or DMSO, 80 °C; d) $Mn(NO_3)_2$, DMF, RT.

ethyl- and 2,6-diisopropyl-*N*-phenyloxamate ligands H_2L^x ($x = 2$ and 3, respectively) were prepared by direct condensation of ethyl chlorooxoacetate with the corresponding aniline derivative in THF (Scheme 2a), as reported earlier for 2,6-dimethyl-*N*-phenyloxamate ligand H_2L^1.[11b] They were isolated as ethyl ester derivatives $HEtL^x$ ($x = 1$–3) in excellent yields (ca. 90–95 %). In the second step cationic mononuclear copper(II) complexes of L^x ($x = 2$ and 3) were synthesised as their sodium salts with general formula $Na_2[Cu(L^x)_2]\cdot q H_2O$ ($q = 2$ and 4), as reported earlier for $Na_2[Cu(L^1)_2]\cdot 4H_2O$.[11b] They were obtained in very good yields (ca. 80–85 %) by deprotonation and hydrolysis of the corresponding proligand $HEtL^x$ with NaOH in water, and subsequent addition of a stoichiometric amount of $Cu(NO_3)_2\cdot 3H_2O$ (Scheme 2b). In a third step, the corresponding heterobimetallic chain compounds of general formula $[MCu(L^x)_2(DMF)_2]\cdot p\,DMF\cdot q\,H_2O$ [$p = 0$–1, $q = 0$–2.5; M = Mn (**1a**–**3a**) and Co (**1b**–**3b**) with $x = 1$–3] and $[MCu(L^x)_2(DMSO)_2]\cdot p\,DMSO\cdot q\,H_2O$ [$p = 0$–1, $q = 0$–2.5; M = Mn (**2c** and **3c**) and Co (**2d** and **3d**) with $x = 2$ and 3] were synthesised as reported earlier for $[MnCu(L^1)_2(DMSO)_2]$ (**1c**) and $[CoCu(L^1)_2(DMSO)_2]\cdot DMSO$ (**1d**).[11b] They were obtained as polycrystalline solids from the reaction of the corresponding sodium salt of the mononuclear copper(II)–L^x ($x = 1$–3) precursor and the nitrate salt of the Mn^{II} or Co^{II} ions in hot DMF or DMSO in good yields (ca. 65–80 and 65–75 %, respectively) (Scheme 2c). Single crystals of the manganese(II)–copper(II) chain compounds **2a** and **3a** were grown by slow diffusion in H-shaped tubes of DMF solutions containing $Mn(NO_3)_2\cdot 4H_2O$ in one arm and $Na_2[Cu(L^x)_2]\cdot 4H_2O$ ($x = 2$ and 3, respectively) in the other at room temperature (Scheme 2d).

The chemical identity of the ligands, the mononuclear copper(II) complexes and the heterobimetallic chain compounds was determined by elemental analysis (C, H, N, S), and ^{1}H NMR and IR spectroscopy (see the Experimental Section). The structures of **2a** and **3a** were further confirmed by single-crystal X-ray diffraction with synchrotron radiation. Crystallographic data for **2a** and **3a** are summarised in Table 1.

Table 1. Crystallographic data for **2a** and **3a**.

	2a	**3a**
formula	$C_{30}H_{40}CuMnN_4O_8$	$C_{37}H_{57}CuMnN_5O_{10}$
M_r [g mol^{-1}]	703.14	850.34
crystal system	monoclinic	monoclinic
space group	*C*2/*c*	*C*2/*c*
a [Å]	13.2213(14)	20.189(4)
b [Å]	13.4991(14)	19.672(4)
c [Å]	19.0033(16)	13.110(3)
β [°]	99.122(6)	113.56(3)
V [Å^3]	3348.6(4)	4772.9(16)
Z	4	4
ρ_{calcd} [g cm^{-3}]	1.395	1.181
F(000)	1464	1784
μ [mm^{-1}]	1.064	0.761
T [K]	100(2)	100(2)
reflns collected	17797	37190
independent reflns (R_{int})	2723	4699
obsd reflns [$I > 2\sigma(I)$]	2459	4491
data/restraints/parameters	2723/0/202	4699/5/235
R_1[a] [$I > 2\sigma(I)$] (all)	0.1021 (0.1074)	0.1248 (0.1263)
wR_2[b] [$I > 2\sigma(I)$] (all)	0.3000 (0.3055)	0.4237 (0.4289)
S[c]	1.046	2.265

[a] $R_1 = \Sigma(|F_o| - |F_c|)/\Sigma|F_o|$. [b] $wR_2 = [\Sigma w(F_o^2 - F_c^2)^2/\Sigma w(F_o^2)^2]^{1/2}$. [c] $S = [\Sigma w(|F_o| - |F_c|)^2/(N_o - N_p)]^{1/2}$.

Description of the structures

*[MnCu(L^2)$_2$(DMF)$_2$] (**2a**)*: Compound **2a** consists of neutral oxamato-bridged manganese(II)–copper(II) zigzag chains (Figure 1). Within each chain, the bis(oxamato)copper(II) entity acts as a bis-bidentate ligand through the *cis* carbonyl-oxygen atoms toward *cis*-bis(dimethylformamide)manganese(II) units (Figure 1a). This situation is similar to that reported earlier for $[CoCu(L^1)_2(H_2O)_2]$, but contrasts with that of $[CoCu(L^4)_2(H_2O)_2]\cdot 2H_2O$ (L^4 = *N*-2,4,6-trimethylphenyloxamate), in which *cis* and *trans* coordination of the two water molecules to the cobalt atoms leads to zigzag and

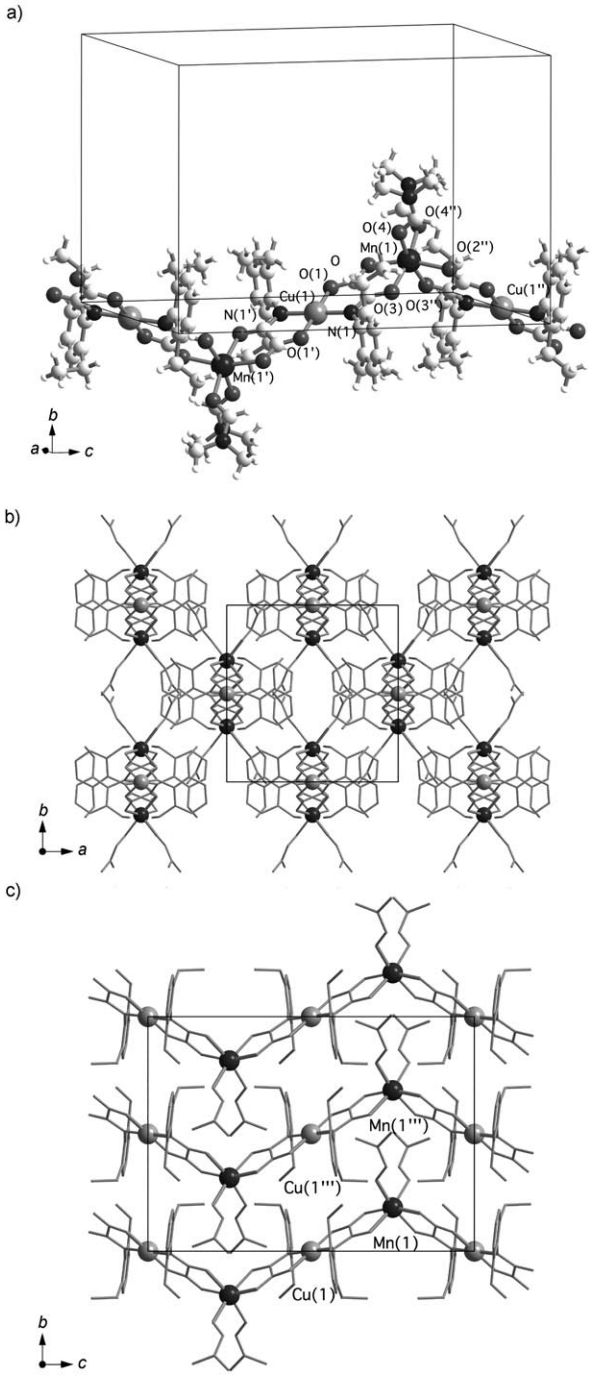

Figure 1. a) View of a fragment of the chain of **2a** with the atom numbering for the metal coordination environments. b), c) Crystal packing of the chains of **2a** along the [001] and [100] directions, respectively. Hydrogen atoms are omitted for clarity [symmetry codes: (′) = 1−*x*, −*y*, 1−*z*; (″) = 1−*x*, *y*, 3/2−*z*; (‴) = −1/2+*x*, 1/2+*y*, *z*].

linear chain structures, respectively.[11a,b] Because of the *cis* conformation of the octahedral Mn atoms in **2a**, two different propeller enantiomers (Δ and Λ) exist, and thus their regular alternation along the chain leads to a global achiral zigzag chain structure. Instead, a chiral helical chain structure would result from a regular alternation of identical isomers (Δ or Λ), like that observed for [CoCu(binaba)-$(DMF)_2$]·DMF [binaba = (*M*)-1,1′-binaphthalene-2,2′-bis-(oxamate)].[11c] Selected bond lengths and angles for **2a** are summarised in Table 2.

Table 2. Selected bond lengths [Å] and angles [°] for **2a**.[a,b]

Cu(1)−N(1)	1.984(5)	Cu(1)−O(1)	1.909(5)
Mn(1)−O(2)	2.187(5)	Mn(1)−O(3)	2.163(5)
Mn(1)−O(4)	2.137(7)		
N(1)-Cu(1)-O(1)	85.9(2)	N(1)-Cu(1)-N(1′)	180.0
N(1)-Cu(1)-O(1′)	94.1(2)	O(1)-Cu(1)-O(1′)	180.0
O(2)-Mn(1)-O(3)	76.50(17)	O(2)-Mn(1)-O(4)	97.6(2)
O(2)-Mn(1)-O(2″)	162.5(3)	O(2)-Mn(1)-O(3″)	92.03(18)
O(2)-Mn(1)-O(4″)	95.4(2)	O(3)-Mn(1)-O(4)	89.3(2)
O(3)-Mn(1)-O(3″)	98.6(3)	O(3)-Mn(1)-O(4″)	168.8(2)
O(4)-Mn(1)-O(4″)	84.1(4)		

[a] Estimated standard deviations are given in parentheses. [b] Symmetry codes: (′) = 1−*x*, −*y*, 1−*z*; (″) = 1−*x*, *y*, 3/2−*z*.

The twofold-symmetry-related Cu(1) and Cu(1″) atoms in **2a** have a four-coordinate square-planar [CuN_2O_2] environment formed by two amidate-nitrogen and two carboxylate-oxygen atoms from the two L^2 ligands in a *trans* arrangement [Cu(1)−N(1) = 1.984(5) and Cu(1)−O(1) = 1.909(5) Å]. The tetrahedral twist angle (τ) at the copper atom is strictly 0.0° for symmetry reasons. The oxamato groups are almost coplanar with the metal basal plane [dihedral angle = 2.8(4)°], whereas the phenyl ring of each L^2 ligand is approximately perpendicular to the oxamato group [dihedral angle = 72.7(3)°] to prevent steric repulsions between the ethyl substituents and the carbonyl-oxygen atoms. More likely, the alternative *cis* arrangement of the L^2 ligands is precluded because of steric hindrance between the 2,6-diethyl-substituted phenyl groups.

The centrosymmetrically related Mn(1) and Mn(1′) atoms have a six-coordinate octahedral [MnO_6] environment. The equatorial plane is defined by two carbonyl-oxygen atoms from the two *cis*-dimethylformamide molecules [Mn(1)−O(4) = 2.137(7) Å] and two carbonyl-oxygen atoms from the amidate groups of the two L^2 ligands [Mn(1)−O(3) = 2.163(5) Å], whereas two carbonyl oxygen-atoms from the carboxylate groups of the two L^2 ligands [Mn(1)−O(2) = 2.187(5) Å] occupy the axial positions. The trigonal twist angle (θ) at the manganese atom is 55.0(4)°, a value which reflects a slight distortion of the octahedral metal environment (θ = 60°) toward trigonal prismatic (θ = 0°) (a so-called Bailar twist). This situation is likely explained by the steric hindrance between the two *cis*-coordinated dimethylformamide molecules.

In the crystal lattice, the zigzag chains of **2a** running parallel to the *c* axis are well separated from each other because of the effective shielding of the 2,6-diethyl-substituted phenyl groups and the *cis*-coordinated dimethylformamide molecules in the *ab* plane (Figure 1b). The adjacent chains related by a simple translation along the [110] direction exhibit a zipper-type close packing (Figure 1c). The intrachain Mn(1)···Cu(1) distance across the oxamato bridge is

5.3761(7) Å, whereas the shortest interchain Mn(1)···Mn(1^{III}) and Cu(1)···Cu(1^{III}) separations are 9.4475(16) Å.

*[MnCu(L^3)$_2$(DMF)$_2$]·DMF·H_2O (**3a**)*: Compound **3a** is made up of neutral oxamato-bridged manganese(II)–copper(II) zigzag chains, together with dimethylformamide and water molecules of crystallisation (Figure 2). As in **2a**, the bis(oxamato)copper(II) entity acts as a bis-bidentate ligand through the *cis* carbonyl oxygen-atoms toward *cis*-bis(dimethylformamide)manganese(II) units to give an achiral zigzag chain structure with alternating propeller chiralities (Δ and Λ) for the octahedral Mn atoms along the chain (Figure 2a). Selected bond lengths and angles for **3a** are summarised in Table 3.

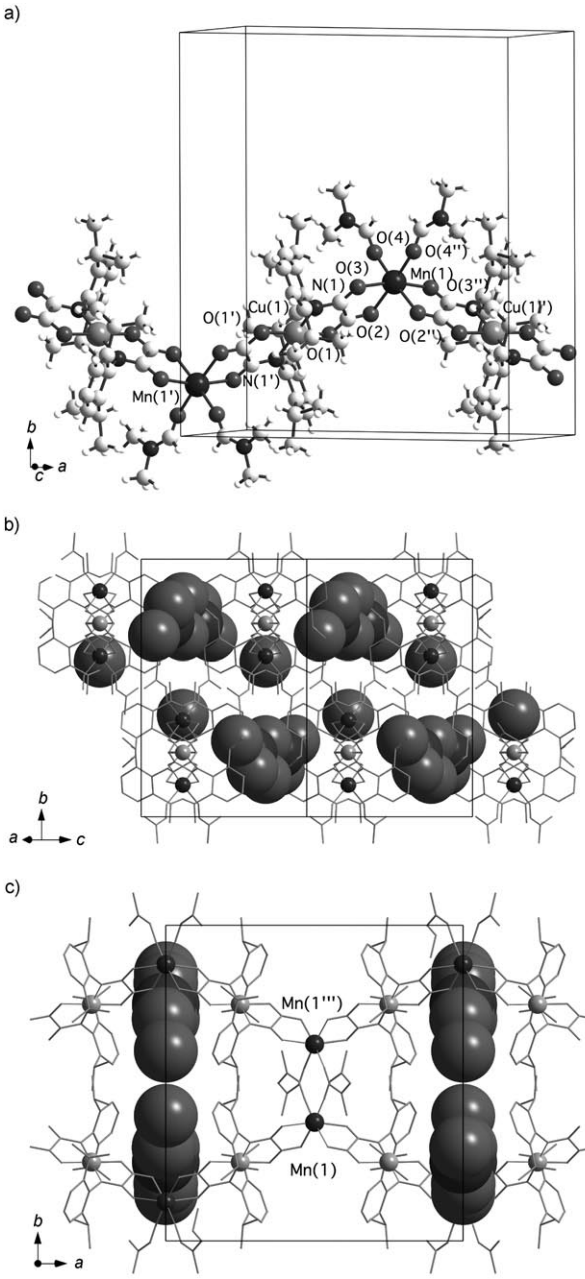

Figure 2. a) View of a fragment of the chain of **3a** with the atom numbering for the metal coordination environments. b), c) Crystal packing of the chains of **3a** along the [101] and [001] directions, respectively. Atoms of the uncoordinated dimethylformamide and water molecules of crystallisation are shown as large spheres with arbitrary radii. Hydrogen atoms are omitted for clarity [symmetry codes: (′) = 1/2−*x*, 1/2−*y*, 1−*z*; (″) = −*x*, *y*, 1/2−*z*; (‴) = 1/2+*x*, 1/2+*y*, *z*].

Table 3. Selected bond lengths [Å] and angles [°] for **3a**.[a,b]

Cu(1)−N(1)	1.934(3)	Cu(1)−O(1)	1.949(4)
Mn(1)−O(2)	2.206(3)	Mn(1)−O(3)	2.150(3)
Mn(1)−O(4)	2.138(3)		
N(1)-Cu(1)-O(1)	84.76(14)	N(1)-Cu(1)-N(1′)	180.0
N(1)-Cu(1)-O(1′)	95.24(13)	O(1)-Cu(1)-O(1′)	180.0
O(2)-Mn(1)-O(3)	76.81(10)	O(2)-Mn(1)-O(4)	87.54(18)
O(2)-Mn(1)-O(2″)	92.31(19)	O(2)-Mn(1)-O(3″)	93.54(11)
O(2)-Mn(1)-O(4″)	174.11(13)	O(3)-Mn(1)-O(4)	92.16(14)
O(3)-Mn(1)-O(3″)	166.20(15)	O(3)-Mn(1)-O(4″)	97.32(13)
O(4)-Mn(1)-O(4″)	93.2(3)		

[a] Estimated standard deviations are given in parentheses. [b] Symmetry codes: (′) = 1/2−*x*, 1/2−*y*, 1−*z*; (″) = −*x*, *y*, 1/2−*z*.

The twofold-symmetry-related Cu(1) and Cu(1″) atoms in **3a** have a four-coordinate square-planar [CuN_2O_2] environment formed by two amidate-nitrogen and two carboxylate-oxygen atoms from the two L^3 ligands in a *trans* arrangement [Cu(1)−N(1) = 1.934(3) and Cu(1)−O(1) = 1.949(4) Å]. As in **2a**, the τ value at the copper atom is strictly 0.0° for reasons of symmetry, and the oxamato groups from each L^3 ligand are also coplanar with the metal basal plane [dihedral angle = 2.2(3)°]. The phenyl ring and the oxamato group from each L^3 ligand are however much closer to perpendicularity [dihedral angle = 79.8(3)°] than in **2a**, and this reflects the larger steric hindrance of the isopropyl substituents compared to the ethyl ones.

The centrosymmetrically related Mn(1) and Mn(1′) atoms have a six-coordinate octahedral [MnO_6] environment formed by four carbonyl-oxygen atoms from the two *cis*-dimethylformamide molecules [Mn(1)−O(4) = 2.138(3) Å] and the carboxylate groups of the two L^3 ligands [Mn(1)−O(2) = 2.206(3) Å] defining the equatorial plane and two carbonyl-oxygen atoms from the amidate functions of the two L^3 ligands [Mn(1)−O(3) = 2.150(3) Å] occupying the axial positions. The θ value at the manganese atom of 54.4(4)° is similar to that found in **2a**, and thus reflects a slight trigonal distortion of the octahedral environment.

In the crystal lattice, the zigzag chains of **3a** running parallel to the [101] direction are well separated from each other because of the effective shielding of the 2,6-diisopropyl-substituted phenyl groups and the *cis*-coordinated dimethylformamide molecules in the *ab* plane (Figure 2b). The packing of adjacent chains related by a glide translation along the *b* axis leads to narrow pores along the *c* axis that are occupied by dimethylformamide and water molecules of crystallisation (Figure 2c). The value of 5.4002(17) Å for the intrachain Mn(1)···Cu(1) distance across the oxamato bridge is close to that of **2a**, and thus reflects the fact that the individual chains are very similar. The value of 8.1649(14) Å for

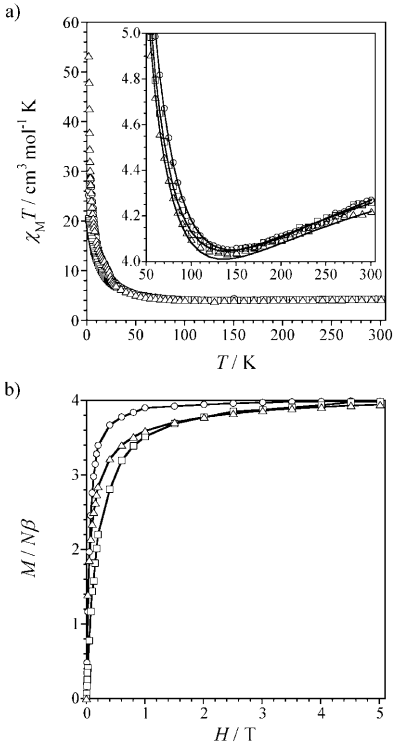

Figure 3. a) Temperature dependence of $\chi_M T$ for **1a** (○), **2a** (□) and **3a** (△) under an applied magnetic field of 1 T ($T \geq 50$ K) and 100 G ($T < 50$ K). Inset: The $\chi_M T$ minima for **1a** (○), **2a** (□) and **3a** (△). The solid lines are the best-fit curves (see text). b) Field dependence of M for **1a** (○), **2a** (□) and **3a** (△) at 2.0 K. The solid lines are guides for the eye.

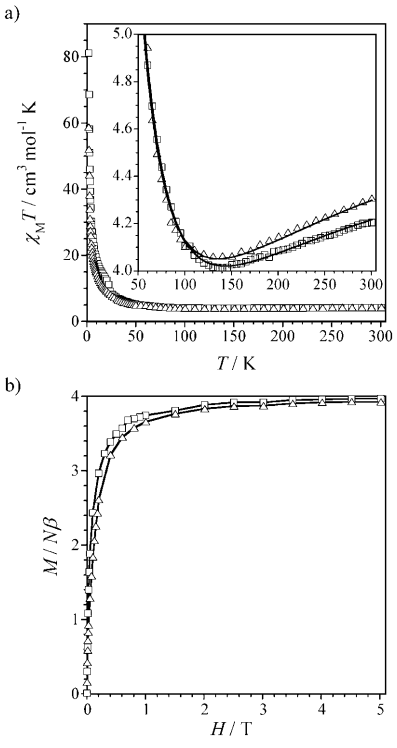

Figure 4. a) Temperature dependence of $\chi_M T$ for**2c** (□) and **3c** (△) under an applied magnetic field of 1 T ($T \geq 50$ K) and 100 G ($T < 50$ K). Inset: The $\chi_M T$ minima for **2c** (□) and **3c** (△). The solid lines are the best-fit curves (see text). b) Field dependence of M for **2c** (□) and **3c** (△) at 2.0 K. The solid lines are guides for the eye.

the shortest interchain Mn(1)···Mn(1‴) separation is, however, smaller than that of **2a**, despite both the larger size of the isopropyl substituents compared to the ethyl ones and the presence of additional dimethylformamide and water molecules of crystallisation. This fact reflects the striking differences in the crystal packing of the individual chains in the two compounds.

Static magnetic properties

Manganese(II)–copper(II) chains: The dc magnetic properties of **1a**–**3a** in the form of $\chi_M T$ versus T plots, in which χ_M is the magnetic susceptibility per MnCu pair and T is the temperature, are similar to those of **2c** and **3c** (Figures 3a and 4a, respectively). The $\chi_M T$ values at room temperature vary in the narrow range of 4.20–4.30 cm^3 mol^{-1} K, and are lower than expected for the sum of a square-planar Cu^{II} ion [$S_{Cu}=1/2$; $\chi_M T=(N\beta^2 g_{Cu}{}^2/3k_B)S_{Cu}(S_{Cu}+1)=0.40$ cm^3 mol^{-1} K with $g_{Cu}=2.1$] and an octahedral high-spin Mn^{II} ion [$S_{Mn}=5/2$; $\chi_M T=(N\beta^2 g_{Mn}{}^2/3k_B)S_{Mn}(S_{Mn}+1)=4.35$ cm^3 mol^{-1} K with $g_{Mn}=2.0$] magnetically isolated. Upon cooling, $\chi_M T$ decreases to attain a minimum around 140 K (inset of Figures 3a and 4a), which is characteristic of ferrimagnetic $Mn^{II}Cu^{II}$ chains with a relatively large intrachain antiferromagnetic interaction between the Mn^{II} and Cu^{II} ions through the oxamato bridge.[17] The $\chi_M T$ value then increases to reach maximum values in the range of 20.4–81.0 cm^3 mol^{-1} K at 2.0 K under a dc magnetic field of 100 G. The lack of a maximum in the χ_M versus T plot (data not shown) allows us to rule out the occurrence of a 3D long-range antiferromagnetic order of the magnetically well-isolated $Mn^{II}Cu^{II}$ chains, as revealed by the crystal structures of **2a** and **3a**.

The M versus H plots for **1a**–**3a** at 2.0 K, in which M is the magnetisation per MnCu pair and H the applied magnetic field, are also similar to those of **2c** and **3c** (Figures 3b and 4b, respectively). The values of M in the range of 3.93–3.99 $N\beta$ at 5.0 T are consistent with that calculated for the saturation magnetisation of an $S=2$ state resulting from the antiparallel alignment of the spins of Mn^{II} ($S_{Mn}=5/2$) and Cu^{II} ($S_{Cu}=1/2$) ions along the chain [$M_s=(g_{Mn}S_{Mn}-g_{Cu}S_{Cu})N\beta=3.90\,N\beta$ with $g_{Mn}=2.0$ and $g_{Cu}=2.1$]. Moreover, the magnetisation isotherms show fast saturation with about 90 % of the maximum M values being reached at a field of 1.0 T. This reveals a strong short-range correlation along the chain because of the relatively large antiferromagnetic coupling between the Mn^{II} and Cu^{II} ions across the oxamato bridge.

The magnetic susceptibility data of **1a**–**3a**, **2c** and **3c** were analysed by using the one-dimensional model developed by Kahn et al. for $Mn^{II}Cu^{II}$ chains, in which the Mn^{II} and Cu^{II} ions are treated as classic ($S_{Mn}=5/2$) and quantum ($S_{Cu}=1/2$) spins, respectively.[17a] In this model, the spin Hamiltonian is expressed by Equation (1), in which i runs over the MnCu units, J is the magnetic coupling parameter

and g_{Mn} and g_{Cu} are the Landé factors of the Mn^{II} and Cu^{II} ions, respectively.

$$\mathbf{H} = \Sigma_i\{-J\mathbf{S}_{Mn,i}\cdot(\mathbf{S}_{Cu,i}+\mathbf{S}_{Cu,i-1})+(g_{Mn}\mathbf{S}_{Mn,i}+g_{Cu}\mathbf{S}_{Cu,i})\beta H\} \quad (1)$$

The theoretical curves obtained by least-squares fit of the experimental data of **1a**–**3a**, **2c** and **3c** through this model in the temperature range 20–300 K reproduce very well the observed minimum in the $\chi_M T$ versus T plots (solid lines in the insets of Figures 3a and 4a). The magnitude of the intrachain antiferromagnetic coupling between the Cu^{II} and Mn^{II} ions through the oxamato bridge for **2c** and **3c** ($-J=33.3$ and 32.4 cm^{-1}, respectively) is close to that reported for **1c** ($-J=28.2$ cm^{-1}),[11b] and similar to those in **1a**–**3a** ($-J=$ 31.4–35.2 cm^{-1}; Table 4). This fact suggests that the two series of $Mn^{II}Cu^{II}$ chains have similar structures despite the different nature of the coordinated solvent molecules (DMSO or DMF).

Table 4. Selected dc magnetic data for **1a**–**3a** and **1c**–**3c**.

	$-J$ [cm^{-1}][a]	g_{Mn}[b]	g_{Cu}[b]
1a	35.2	2.00	2.09
2a	32.1	2.00	2.06
3a	31.4	2.00	2.08
1c[c]	28.2	2.00	2.07
2c	33.3	2.00	2.07
3c	32.4	2.00	2.08

[a] Intrachain magnetic coupling parameter [see Eq. (1)]. [b] Landé factor [see Eq. (1)]. [c] Data from ref. [11b].

Cobalt(II)–copper(II) chains: The dc magnetic properties of **1b**–**3b** in the form of $\chi_M T$ versus T plot (χ_M is the magnetic susceptibility per CoCu pair) are similar to those of **2d** and **3d** (Figures 5a and 6a, respectively). At room temperature, the $\chi_M T$ values in the range of 2.07–2.59 $cm^3 mol^{-1} K$ are lower than expected for the sum of a square-planar Cu^{II} ion ($S_{Cu}=1/2$) [$\chi_M T=(N\beta^2 g_{Cu}{}^2/3k_B)S_{Cu}(S_{Cu}+1)=0.40$ $cm^3 mol^{-1} K$ with $g_{Cu}=2.1$] and an octahedral high-spin Co^{II} ion ($S_{Co}=3/2$) with an important orbital contribution ($\chi_M T=(N\beta^2 g_{Co}{}^2/3k_B)S_{Co}(S_{Co}+1)=2.9$ $cm^3 mol^{-1} K$ with $g_{Co}=2.5$) magnetically isolated. Upon cooling, $\chi_M T$ decreases to attain a minimum in the range of 85.5–135.0 K (insets of Figures 5a and 6a), which is typical of ferrimagnetic $Co^{II}Cu^{II}$ chains with a relatively large intrachain antiferromagnetic interaction between the Co^{II} and Cu^{II} ions through the oxamato bridge.[18] Finally, $\chi_M T$ reaches a maximum in the range of 5.5–7.5 K under a dc magnetic field of 100 G due to the magnetic anisotropy and/or saturation effects. The lack of a χ_M maximum allows us to rule out the occurrence of a 3D long-range antiferromagnetic order, and thus suggests that the $Co^{II}Cu^{II}$ chains are magnetically well-isolated from each other, too.

The M versus H plots for **1b**–**3b** at 2.0 K (M is the magnetisation per CoCu pair) are also similar to those of **2d** and **3d** (Figures 5b and 6b, respectively). The M values in the range of 0.99–1.21 $N\beta$ at 5.0 T are consistent with the calculated value of the saturation magnetisation for a partial spin cancellation resulting from the antiparallel alignment of the spins of Co^{II} ($S_{Co}=S_{eff}=1/2$) and Cu^{II} ($S_{Cu}=1/2$) ions [$M_s=(g_{Co}S_{Co}-g_{Cu}S_{Cu})N\beta=1.10N\beta$ with $g_{Co}=4.3$ and $g_{Cu}=$ 2.1]. In fact, the octahedral high-spin Co^{II} ions with an orbitally degenerate $^4T_1$ single-ion ground state ($S_{Co}=3/2$ and $L_{Co}=1$) behave as an effective $S_{eff}=1/2$ spin state because only the ground Kramer's doublet resulting from the spin–orbit coupling is populated at 2.0 K. The magnetisation isotherms show fast saturation with up to 90% of the maximum M value being reached at a field of 0.1 T for **2d**. This reveals a strong short-range correlation along the chain due to the relatively large antiferromagnetic coupling between the Co^{II} and Cu^{II} ions across the oxamato bridge. Moreover, a magnetic hysteresis loop is observed for **2d** at 2.0 K with relatively low values of the coercive field ($H_c=150$ G) and the remanent magnetization ($M_r=0.45$ $cm^3 mol^{-1}$ G; inset of Figure 6b). This is indicative of slow relaxation of the magnetisation within the individual chains or 3D long-range ferromagnetic order between the chains.

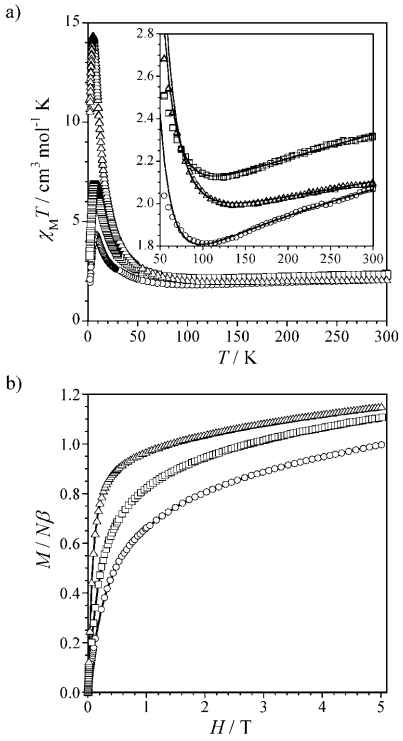

Figure 5. a) Temperature dependence of $\chi_M T$ for **1b** (○), **2b** (□) and **3b** (△) under an applied static field of 1 T ($T \geq 50$ K) and 100 G ($T < 50$ K). Inset: The $\chi_M T$ minima for **1b** (○), **2b** (□) and **3b** (△). The solid lines are the best-fit curves (see text). b) Field dependence of M for **1b** (○), **2b** (□) and **3b** (△) at 2.0 K. The solid lines are guides for the eye.

The magnetic susceptibility data of **1c**–**3c**, **2d** and **3d** were analysed by using the one-dimensional branch chain model developed by Kahn et al. for $Co^{II}Cu^{II}$ chains,[18a] in which the Co^{II} ions are orbitally degenerate ($^4T_1$ ground term). This model assumes that only z components of spin and orbital momenta are coupled and that the applied magnetic field is along the quantization axis. The corresponding

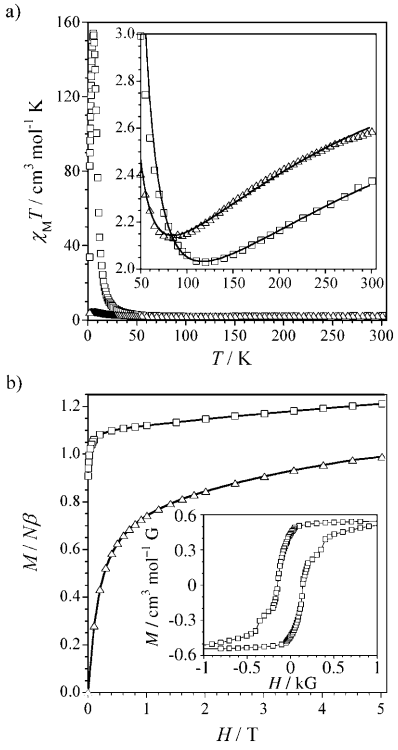

Figure 6. a) Temperature dependence of $\chi_M T$ for **2d** (□) and **3d** (△) under an applied static field of 1 T ($T \geq 50$ K) and 100 G ($T < 50$ K). Inset: The $\chi_M T$ minima for **2d** (□) and **3d** (△). The solid lines are the best-fit curves (see text). b) Field dependence of M for **2d** (□) and **3d** (△) at 2.0 K. Inset: The hysteresis loop of **2d** (□). The solid lines are guides for the eye.

Hamiltonian is then expressed by Equation (2), in which i runs over the CoCu units, J and J' are the isotropic magnetic exchange and effective spin–orbit coupling parameters respectively, κ is the orbital reduction, Δ is the splitting of the T_1 orbital term of the Co^{II} ion in a singlet and doublet orbital terms due to an axial symmetry and g_{Co} and g_{Cu} are the Landé factors of the Co^{II} and Cu^{II} ions, respectively.

$$\mathbf{H} = \Sigma_i \{ -J\mathbf{S}_{Co,i(z)} \cdot (\mathbf{S}_{Cu,i(z)} + \mathbf{S}_{Cu,i-1(z)}) + J'\mathbf{L}_{Co,i(z)} \cdot \mathbf{S}_{Co,i(z)} + \Delta \mathbf{L}_{Co,i(z)}{}^2 + (g_{Co}\mathbf{S}_{Co,i(z)} + g_{Cu}\mathbf{S}_{Cu,i(z)} + \kappa \mathbf{L}_{Co,i(z)})\beta H_{(z)} \} \quad (2)$$

The theoretical curves obtained by least-squares fit of the experimental data of **1c–3c**, **2d** and **3d** through this model in the temperature range 50–300 K reproduce quite well the observed minimum in the $\chi_M T$ versus T plots (solid lines in the insets of Figures 5a and 6a). The magnitude of the intrachain antiferromagnetic coupling between Cu^{II} and Co^{II} ions through the oxamato bridge for **1b–3b** ($-J = 41.2$–46.4 cm^{-1}) is within the range of those found for **1d** and **2d** ($-J = 40.5$ and 48.0 cm^{-1}, respectively), but it is somewhat larger than that found in **3d** ($-J = 33.4$ cm^{-1}; Table 5). This fact suggests that the Cu^{II} ion in **3d** is not ideally square planar but slightly tetrahedrally distorted, as previously reported for the aforementioned chain compound [CoCu(binaba)$(DMF)_2$]·DMF ($-J = 28.9$ cm^{-1}).[11c] This situation would lead to a poorer overlap of the magnetic orbitals of the Cu^{II} and Co^{II} ions through the σ in-plane orbital pathway of the oxamato bridge, and thus to a smaller intrachain antiferromagnetic coupling.

Table 5. Selected dc magnetic data for **1b–3b** and **1d–3d**.

	$-J$ [cm^{-1}][a]	g_{Co}[b]	g_{Cu}[b]	$-\lambda$ [cm^{-1}][c]	κ[d]	Δ [cm^{-1}][e]
1b	41.2	2.17	2.12	129	0.97	280
2b	42.7	2.25	2.08	123	0.90	352
3b	46.4	2.26	2.08	121	0.97	317
1d[f]	40.5	2.30	2.07	107	0.97	719
2d	48.0	2.19	2.03	121	0.90	758
3d	33.4	2.24	2.03	150	0.77	675

[a] Intrachain magnetic coupling parameter [see Eq. (2)]. [b] Landé factor [see Eq. (2)]. [c] Spin–orbit coupling parameter with $A = 3/2$ [see Eq. (2)]. [d] Orbital reduction parameter [see Eq. (2)]. [e] Axial orbital splitting parameter [see Eq. (2)]. [f] Data from ref. [11b].

The effective spin–orbit coupling (J') can be related to the spin–orbit coupling parameter (λ) of the $^4T_1$ ground term of the Co^{II} ion in octahedral symmetry through the expression $J' = -A\kappa\lambda$, in which κ is the reduction of the orbital momentum caused by the ligand delocalization of the unpaired electrons (nephelauxetic effect) and A is a crystal field parameter ($A = 3/2$ and 1 for the weak and strong crystal-field limits, respectively).[18c] The calculated values of the orbital reduction and spin–orbit coupling parameters of the Co^{II} ion in **1b–3b** and **1d–3d** ($\kappa = 0.77$–0.97 and $-\lambda = 107$–150 cm^{-1} with $A = 3/2$; Table 5) thus reflect the degree of the metal–ligand covalency ($\kappa = 1.0$ and $\lambda = -180$ cm^{-1} for the free ion). On the other hand, the larger magnitude of the local axial octahedral distortion parameter (Δ) of the Co^{II} ion in **1d–3d** ($\Delta = 675$–758 cm^{-1}) compared to those in **1b–3b** ($\Delta = 280$–352 cm^{-1}; Table 5) likely reflects a greater anisotropy of the DMSO derivatives (**1d–3d**) when compared to the DMF ones (**1b–3b**).

Dynamic magnetic properties

Manganese(II)–copper(II) chains: The ac magnetic properties of **1a–3a**, **2c** and **3c** in the form of χ_M' and χ_M'' versus T plots (χ_M' and χ_M'' are the in-phase and out-of-phase magnetic susceptibilities per MnCu pair, respectively) at different frequencies (ν) of a 1 G oscillating field show neither evidence of slow magnetic relaxation effects within the individual chains nor 3D long-range ferromagnetic order between the chains. In fact, no χ_M'' signals were observed above 2.0 K for these two series of manganese(II)–copper(II) chain compounds (data not shown). This is likely due to the magnetically isotropic character of the octahedral high-spin Mn^{II} ion with a $^6A_1$ single-ion ground state and the very good isolation of the $Mn^{II}Cu^{II}$ chains, as revealed by the crystal structures of **2a** and **3a**.

Cobalt(II)–copper(II) chains: The ac magnetic properties of **1b–3b**, **2d** and **3d** in the form of the χ_M' and χ_M'' versus T plots (χ_M' and χ_M'' are the in-phase and out-of-phase magnetic susceptibilities per CoCu pair, respectively) at differ-

ent frequencies (ν) of a 1 G oscillating field show evidence of slow magnetic relaxation effects for **2d** and **3d** (Figures 7 and 8, respectively, and Figures S1 and S2, respectively, in

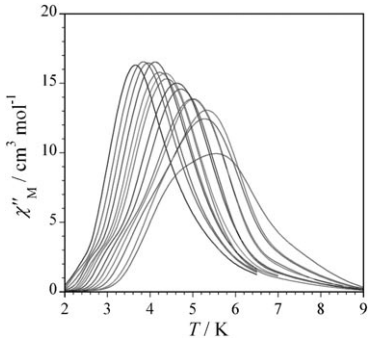

Figure 7. Temperature dependence of χ_M'' for **2d** under zero applied static field at different frequencies of a ± 1 G oscillating field in the range of 0.1–1000 Hz.

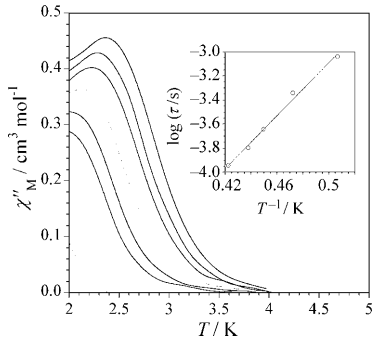

Figure 8. Temperature dependence of χ_M'' for **3d** under zero applied static field at different frequencies of a ± 1 G oscillating field in the range of 10–1000 Hz. Inset: The inset shows the Arrhenius plot for **3d**. The solid line is the best-fit curve

the Supporting Information) but also for **1b–3b** (Figures S3–S5, Supporting Information). Thus, χ_M'' becomes nonzero below 4.0 K for **1b–3b**, but no maxima are observed above 2.0 K (Figures S3b–S5b, Supporting Information). The χ_M'' value also becomes nonzero below 10.0 and 4.0 K for **2d** and **3d**, respectively, and it shows maxima between 5.6 ($\nu = 1000$ Hz) and 3.6 K ($\nu = 0.1$ Hz) for **2d**, and between 2.5 ($\nu = 1000$ Hz) and 2.1 K ($\nu = 350$ Hz) for **3d** (Figures 7 and 8, respectively), as previously observed for **1d**, which shows a unique maximum at 2.1 K for the highest applied frequency ($\nu = 1000$ Hz).[11b] The relative variation of the temperature of the maximum of χ_M'' with respect to the frequency of the oscillating field is expressed by the so-called Mydosh parameter (F), defined by Equation (3).[19] The calculated F values of 0.11 (**2d**) and 0.17 (**3d**) are within the range of $0.1 < F < 0.3$ expected for SCMs.

$$F = (\Delta T_{max}/T_{max})/\Delta(\lg \nu) \quad (3)$$

The relaxation time (τ) of the magnetisation for **2d** and **3d**, which can be calculated from the maximum of χ_M'' at a given frequency (ν), at which it is assumed that the switching of the oscillating field matches the relaxation rate of the magnetisation ($1/\tau = 2\pi\nu$), diverges exponentially as in SCMs. Thus, the calculated τ values at T_{max} for **2d** and **3d** follow the Arrhenius law given by Equation (4), characteristic of a thermally activated mechanism (Figure 9 and inset

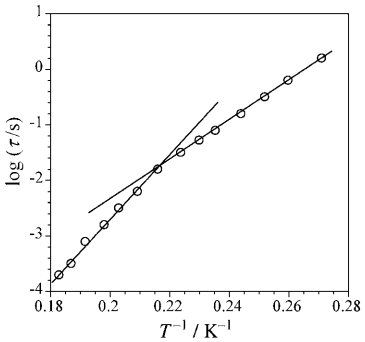

Figure 9. Arrhenius plots for **2d** for $T > 4.5$ K (left) and $T < 4.5$ K (right). The solid lines are best-fit curves (see text).

of Figure 8), but they deviate at higher temperatures ($T \geq 4.5$ K) or higher frequencies for **2d** (Figure 9). The values of the preexponential factor (τ_0) are 3.2×10^{-10} ($T < 4.5$ K) and 3.2×10^{-14} s ($T > 4.5$ K) for **2d** and 2.6×10^{-9} s for **3d**, whereas the values of the energy barrier (E_a) are 24.7 ($T < 4.5$ K) and 37.5 cm^{-1} ($T > 4.5$ K) for **2d** and 7.7 cm^{-1} for **3d** (Table 6). The calculated τ_0 and E_a values for **2d** in the low-

Table 6. Selected ac magnetic data for **2d** and **3d**.

	F[a]	τ_0[b] [s]	E_a[c] [cm^{-1}]	α[d]	χ_S[e] [cm^3 mol^{-1}]	χ_T[f] [cm^3 mol^{-1}]
2d[g]	0.11	3.2×10^{-10}	24.7	0.25	0.18	9.5
	0.11	3.2×10^{-14}	37.5	0.45	25.0	87.2
3d	0.17	2.6×10^{-9}	7.7	0.40	1.9	2.8

[a] Mydosh parameter [see Eq. (3)]. [b] Pre-exponential factor [see Eq. (4)]. [c] Activation energy [see Eq. (4)]. [d] Cole–Cole parameter [see Eq. (5)]. [e] Adiabatic susceptibility [see Eq. (5)]. [f] Isothermal susceptibility [see Eq. (5)].

temperature region and those for **3d** are close to the reported values for the related oxamato-bridged SCMs of formula $[CoCu(L^4)_2(DMSO)_2]\cdot DMSO$ (**4d**; $\tau_0 = 4.0 \times 10^{-9}$ s and $E_a = 38.0$ cm^{-1}) and $[CoCu(L^4)_2(H_2O)_2]\cdot 2H_2O$ (**4e**; $\tau_0 = 2.3 \times 10^{-11}$ and $E_a = 16.3$ cm^{-1}), in which L^4 is the *N*-2,4,6-trimethylphenyloxamate ligand.[11b] However, the calculated E_a value for **2d** in the high-temperature region is larger and the τ_0 value is smaller.[19]

$$\tau = \tau_0 \exp(E_a/k_B T) \quad (4)$$

The χ_M'' versus χ_M' plots (so-called Cole–Cole plots)[20a] at $T = 3.0$–5.0 K for **2d** and at $T = 2.0$ K for **3d** again show the presence of two different relaxation processes for **2d** (Figure 10). This behaviour has already been reported for SMMs,[21] but there are no published examples in the case of

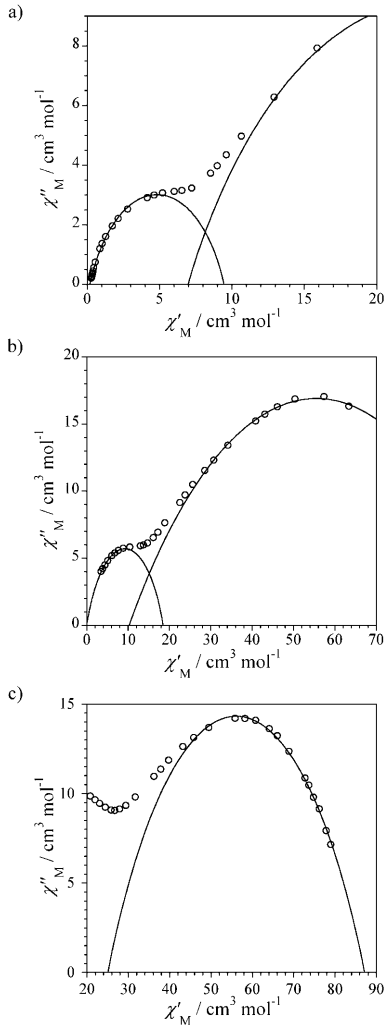

Figure 10. Cole–Cole plots for **2d** at a) 3, b) 4 and c) 5 K. The solid lines are best-fit curves (see text).

SCMs. So, although the Cole–Cole plot of **3d** follows the shape of a semicircle characteristic of a single relaxation process (Figure 11), that of **2d** exhibits unprecedented pair-fused semicircles (Figure 10). The theoretical curve obtained by least-squares fit of the experimental data of **3d** through a generalised Debye model given by Equation (5) reproduces the observed semicircle in the Cole–Cole plot (solid line in Figure 11). In **2d**, the theoretical curves obtained by considering each relaxation process separately provide a rough approach to the two possible semicircles related to each process (solid lines in Figure 10). The coexistence of both semicircles occurs at $T=4$ K (Figure 10b), that is, both relaxation regimes have similar weights at this temperature. However, at lower ($T=3$ K) or higher ($T=5$ K) temperatures, one of the processes becomes dominant, in agreement with the change of the slope in the Arrhenius law at about 4.5 K (Figure 9).

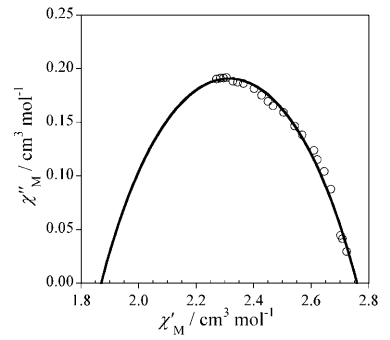

Figure 11. Cole–Cole plot for **3d** at 2 K. The solid line is the best-fit curve (see text).

The calculated values of the Cole–Cole parameters (α), which determine the width of the τ distribution, the adiabatic (χ_S) and isothermal (χ_T) susceptibilities for **2d** and **3d**, are given in Table 6. The α value for **3d** ($\alpha=0.40$) is somewhat greater than expected for a SCM ($\alpha=0$ for an ideal Debye model with a single relaxation time). In general, these large values ($0<\alpha<0.5$) are commonly attributed to the existence of interchain magnetic interactions. However, for **2d** a value of $\alpha=0.45$ is observed for $T\geq 4.5$ K, which is greater than that observed for $T\leq 4.5$ K ($\alpha=0.25$). Clearly, this large value of α cannot be attributed to interchain magnetic interactions, because these interactions would increase at lower temperatures, increasing the value of α, in contrast to what is observed. Very large values of α indicate a broad distribution of relaxation times.[19] Thus, this unique dual regime for the slow dynamics of the magnetisation in **2d** is currently under investigation.

$$\chi''(\chi)=\frac{\chi_T-\chi_S}{2\tan[(1+\alpha)\pi/2]}\left\{(\chi'-\chi_S)(\chi_T-\chi')+\frac{(\chi_T-\chi_S)^2}{4\tan^2[(1-\alpha)\pi/2]}\right\}^{1/2} \quad (5)$$

Conclusion

The present work and Part 1 of this series[11b] are illustrative examples of the ligand design strategy for the rational synthesis of a new family of heterobimetallic SCMs from the self-assembly of bis-bidentate square-planar copper(II) complexes with sterically hindered, polyalkyl-substituted phenyloxamate bridging ligands and transition-metal ions, such as manganese(II) and cobalt(II), with coordinated solvent molecules and/or solvent molecules of crystallisation, such as dimethylformamide, dimethyl sulfoxide or water (see Scheme 1). Thus, systematic variation of the size, number and position of the alkyl substituents (R′=Me, Et and *i*Pr with $n=1$–3) in the Cu^{II}–L^x ($x=1$–4) precursor and the changes in the nature of the Co^{II}-coordinated solvent molecules or solvent molecules of crystallisation (S=DMF, DMSO and H_2O) are clearly reflected in both the static and dynamic magnetic behaviour of the corresponding oxamato-bridged $Co^{II}Cu^{II}$ SCMs, as summarised in Table 7.

Overall, the blocking temperature for the series of $Co^{II}Cu^{II}$ chains with coordinated DMSO ($T_B=2.1$–5.6 K for **1d**–**4d**) and H_2O ($T_B=2.2$ K for **4e** and $T_B<2.0$ K for **1e**) are higher than those with coordinated DMF ($T_B<2.0$ K for

Table 7. Summary of dc and ac magnetic data for **1b–3b**, **1d–3d** and related oxamato-bridged $Co^{II}Cu^{II}$ SCMs.

	$-J$ [cm^{-1}][a]	Δ [cm^{-1}][b]	T_B [K][c]	E_a [cm^{-1}][d]
1b	41.2	280	<2.0	
2b	42.7	352	<2.0	
3b	46.4	317	<2.0	
1d[e]	40.5	719	2.1	
2d	48.0	758	5.6	24.7 (37.5)[f]
3d	33.4	675	2.3	7.7
4d[e]	44.3	710	3.3	38.0
1e[e]	45.8	692	<2.0	
4e[e]	35.0	610	2.2	16.3

[a] Intrachain magnetic coupling parameter [see Eq. (2)]. [b] Axial orbital splitting parameter [see Eq. (2)]. [c] Blocking temperature defined as the temperature of the maximum of χ_M'' at a given frequency ($T_B = T_{max}$ at $\nu = 1000$ Hz). [d] Activation energy [see Eq. (4)]. [e] Data from ref. [11b]. [f] The activation energy for the second relaxation process is given in parentheses.

1b–3b; Table 7). This is most likely due to the presence of DMSO and H_2O molecules of crystallisation for **1d–4d** and **4e**, respectively, which leads to better isolation of the chains compared to their analogues **1b–3b** and **1e**, for which only coordinated DMF or H_2O molecules, respectively, are present. However, the values of the blocking temperature along the former series of cobalt(II)–copper(II)–L^x chain compounds vary in the order **1d** < **3d** < **4d** < **2d**, which is not the expected trend from the steric hindrance of the polyalkyl-substituted phenyloxamate bridging ligands according to $L^1 < L^2 < L^3 < L^4$ sequence. In this regard, compound **2d** reported herein has the highest T_B value among this family of oxamato-bridged SCMs (Figure 12). It thus appears that the interchain interactions depend on subtle crystal-packing effects that are difficult to control by the synthetic chemist, as revealed by the crystal structures of the manganese(II)–copper(II)–L^x analogues **2a** and **3a**, which show longer interchain metal–metal separations for L^2 than for L^3 despite the smaller steric hindrance of the ethyl substituents compared to the isopropyl ones.

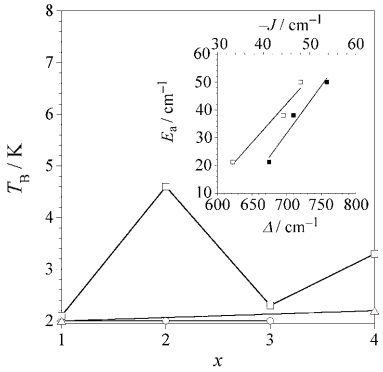

Figure 12. Variation in the blocking temperature (T_B) for the series of oxamato-bridged cobalt(II)–copper(II)–L^x ($x = 1$–4) chain compounds with dimethylformamide (○), dimethyl sulfoxide (□) and water (△) as coordinated solvent molecules (data from Table 7). The solid lines are guides for the eye. Inset: dependence of the activation energy (E_a) for the magnetisation reversal of the intrachain magnetic coupling (□) and the axial orbital splitting (■) for **2d–4d** (data from Table 7). The solid lines are best linear-fit curves (see text).

Alternatively, the greater axial orbital splitting of the octahedral high-spin Co^{II} ion with coordinated DMSO [Δ = 675–758 cm^{-1} (**1d–4d**)] and H_2O [Δ = 692 (**1e**) and 610 cm^{-1} (**4e**)] compared to those with coordinated DMF [Δ = 280–352 cm^{-1} (**1b–3b**)] can also explain the observation of SCM behaviour at higher blocking temperatures, given that the intrachain antiferromagnetic coupling is comparable for these series of $Co^{II}Cu^{II}$ chains [$-J$ = 41.2–46.4 (**1b–3b**), 33.4–48.0 (**1d–4d**), 45.8 (**1e**) and 35.0 cm^{-1} (**4e**)]. In fact, the larger the intrachain antiferromagnetic coupling and the local magnetic anisotropy for **2d–4d**, the greater the activation energy to reverse the magnetisation direction (inset of Figure 12), as expected from the simple model developed by Glauber to explain the slow dynamics of the magnetisation for an Ising 1D system.

Experimental Section

Reagents: Nitrate salts of the metals, sodium hydroxide, ethyl chlorooxoacetate and 2,6-dialkylaniline derivatives were purchased from commercial sources and used as received. The ligand $HEtL^1$ and the mononuclear copper(II) complex $Na_2[Cu(L^1)_2]\cdot 2H_2O$ were prepared as previously reported.[11b]

***N*-2,6-Diethylphenyloxamic acid ethyl ester ($HEtL^2$) and *N*-2,6-diisopropylphenyloxamic acid ethyl ester ($HEtL^3$)**: The ethyl esters of the proligands $HEtL^x$ ($x = 2$, 3) were prepared by following the synthetic procedure previously reported for $HEtL^1$.[11b] In a typical preparation, the corresponding 2,6-dialkylaniline derivative (60 mmol) was treated with ethyl chlorooxoacetate (7.0 mL, 60 mmol) in THF (150 mL) at 0 °C under continuous stirring. The resulting solution was heated to reflux for 1 h and the solvent was removed in a rotatory evaporator to afford an oil that solidified when left at RT. The white solid obtained was filtered off, washed with a small amount of diethyl ether and dried under vacuum.

$HEtL^2$: Yield: 95%; ^{1}H NMR ([D$_6$]DMSO): $\delta = 1.10$ (t, 6H; $2CH_3$), 1.32 (t, 3H; CH_3), 2.48 (q, 4H; $2CH_2O$), 4.31 (q, 2H; CH_2O), 7.12 (d, 2H; 3-H and 5-H of C_6H_3), 7.20 (t, 1H; 4-H of C_6H_4), 10.83 ppm (s, 1H; NH); IR (KBr): $\tilde{\nu} = 3238$ (N–H), 3021, 2967 and 2934 (C–H), 1733 and 1692 cm^{-1} (C=O); elemental analysis calcd (%) for $C_{14}H_{19}NO$ (249): C 67.47, H 7.63, N 5.62; found: C 67.27, H 7.41, N 5.72.

$HEtL^3$: Yield: 90%; ^{1}H NMR ([D$_6$]DMSO): $\delta = 1.10$ (d, 12H; CH_3 of $CH(CH_3)_2$), 1.28 (t, 3H; CH_3), 3.98 (h, 2H; CH of $CH(CH_3)_2$), 4.32 (q, 2H; CH_2O), 7.16 (d, 2H; 3-H and 5-H of $C_6H_3N(iPr)_2$), 7.28 (t, 1H; 4-H of $C_6H_3N(iPr)_2$), 10.32 ppm (s, 1H; NH); IR (KBr): $\tilde{\nu} = 3275$ (N–H), 3062, 2963 and 2943 (C–H), 1739 and 1687 cm^{-1} (C=O); elemental analysis calcd (%) for $C_{16}H_{23}NO_3$ (277): C 69.31, H 8.30, N, 5.05; found: C 69.27, H 8.41, N 5.12.

$Na_2[Cu(L^2)_2]\cdot 4H_2O$ and $Na_2[Cu(L^3)_2]\cdot 4H_2O$: The sodium salts of the copper(II)–L^x ($x = 2$, 3) precursors were prepared by following the synthetic procedure reported previously for $Na_2[Cu(L^1)_2]\cdot 2H_2O$.[11b] In a typical experiment, $HEtL^x$ ($x = 2$, 3; 10 mmol) was suspended in water (25 mL) and allowed to react with aqueous NaOH (1.0 g, 25 mmol; 25 mL). $Cu(NO_3)_2\cdot 3H_2O$ (1.21 g, 5 mmol) dissolved in water (25 mL) was added dropwise to the resulting colourless solution at RT under continuous stirring. The resulting deep-green solution was then filtered on paper remove the small amount of solid particles. The solvent was reduced to a quarter of its volume in a rotatory evaporator and a solid separated. The green polycrystalline solid was filtered off, washed with acetone and diethyl ether and dried under vacuum.

$Na_2[Cu(L^2)_2]\cdot 4H_2O$: Yield: 85%; IR (KBr): $\tilde{\nu} = 3391$ (O–H), 3028, 2965 and 2932 (C–H), 1613 and 1583 cm^{-1} (C=O); elemental analysis calcd (%) for $C_{24}H_{34}CuN_2Na_2O_{10}$ (620): C 46.45, H 5.48, N 4.52; found: C 46.43, H 5.41, N, 4.39.

$Na_2[Cu(L^3)_2]\cdot 4H_2O$: Yield: 85%; IR (KBr): $\tilde{\nu}=3420$ (O−H), 3042 and 2963 (C−H), 1647 and 1619 (C=O) cm^{-1}; elemental analysis calcd (%) for $C_{28}H_{25}CuN_2Na_2O_{10}$ (675): C 49.75, H 3.71, N 4.15; found: C 49.13, H 3.56, N 4.19.

$[MnCu(L^1)_2(DMF)_2]$ (1a), $[MnCu(L^2)_2(DMF)_2]$ (2a) and $[MnCu(L^3)_2(DMF)_2]\cdot DMF\cdot H_2O$ (3a): Compounds **1a–3a** were prepared by following a standard synthetic procedure.[11b] In a typical experiment, $Mn(NO_3)_2\cdot 4H_2O$ (0.062 g, 0.25 mmol) was dissolved in hot DMF (10 mL) and added dropwise to a solution of $Na_2[Cu(L^x)_2]\cdot qH_2O$ ($x=1$–3, $q=2$–4; 0.25 mmol) dissolved in hot DMF (10 mL) at 80°C. The resulting dark-green solution was filtered while hot and the filtrate was allowed to stand at RT. After several days, green polycrystalline solids of **1a–3a** appeared, and were filtered off and air-dried. Well-formed tiny deep-green prisms of **2a** and **3a** suitable for X-ray diffraction were obtained by slow diffusion in an H-shaped tube of DMF solutions containing stoichiometric amounts of $Mn(NO_3)_2\cdot 4H_2O$ in one arm and $Na_2[Cu(L^x)_2]\cdot 4H_2O$ ($x=2$, 3) in the other at RT.

1a: Yield: 75%; IR (KBr): $\tilde{\nu}=3431$ (O−H), 2960 and 2921 (C−H), 1603 and 1628 (C=O) cm^{-1}; elemental analysis calcd (%) for $C_{26}MnCuH_{32}N_4O_8$ (647): C 48.26, H 4.98, N 8.66; found: C 47.76, H 4.98, N 8.95.

2a: Yield: 65%; IR (KBr): $\tilde{\nu}=3431$ (O−H), 2960 and 2921 (C−H), 1602 and 1648 cm^{-1} (C=O); elemental analysis calcd (%) for $C_{30}MnCuH_{40}N_4O_8$ (703): C 51.24, H 5.93, N 7.97; found: C 51.25, H 5.71, N 7.95.

3a: Yield: 70%; IR (KBr): $\tilde{\nu}=3423$ (O−H), 2962 and 2929 (C−H), 1603 and 1630 cm^{-1} (C=O); elemental analysis calcd (%) for $C_{37}MnCuH_{55}N_5O_9$ (850): C 52.26, H 6.75, N 8.24; found: C 52.13, H 6.70, N 8.16.

$[CoCu(L^1)_2(DMF)_2]$ (1b), $[CoCu(L^2)_2(DMF)_2]$ (2b) and $[CoCu(L^3)_2(DMF)_2]\cdot 2.5H_2O$ (3b): Compounds **1b–3b** were prepared by following a standard synthetic procedure.[11b] In a typical experiment, $Co(NO_3)_2\cdot 6H_2O$ (0.073 g, 0.25 mmol) was dissolved in hot DMF (10 mL) and added dropwise to a solution of $Na_2[Cu(L^x)_2]\cdot qH_2O$ ($x=1$–3, $q=2$–4; 0.25 mmol) dissolved in hot DMSO (10 mL) at 80°C. The resulting dark-green solution was filtered while hot and the filtrate was allowed to stand at room temperature. After several days, green polycrystalline solids of **1b–3b** appeared, which were filtered off and air-dried.

1b: Yield: 80%; IR (KBr): $\tilde{\nu}=3433$ (O−H), 2939 and 2921 (C−H), 1601 and 1625 cm^{-1} (C=O); elemental analysis calcd (%) for $C_{26}CoCuH_{32}N_4O_8$ (651): C 47.97, H 4.95, N 8.60; found: C 47.08, H 4.89, N 8.59.

2b: Yield: 75%; IR (KBr): $\tilde{\nu}=3448$ (O−H), 2965 and 2934 (C−H), 1601 and 1646 cm^{-1} (C=O); elemental analysis calcd (%) for $C_{30}CoCuH_{40}N_4O_8$ (706): C 50.95, H 5.70, N 7.93; found: C 50.39, H 5.54, N 7.18.

3b: Yield: 75%; IR (KBr): $\tilde{\nu}=3423$ (O−H), 2962 and 2934 (C−H), 1601 cm^{-1} (C=O); elemental analysis calcd (%) for $C_{34}CoCuH_{53}N_4O_{10.5}$ (807): C 50.52, H 6.61, N 6.93; found: C 49.05, H 6.24, N 5.93.

$[MnCu(L^2)_2(DMSO)_2]$ (2c) and $[MnCu(L^3)_2(DMSO)_2]\cdot 0.5DMSO\cdot 2.5H_2O$ (3c): Compounds **2c** and **3c** were prepared by following the synthetic procedure reported previously for $[MnCu(L^1)_2(DMSO)_2]$ (**1c**).[11b] In a typical experiment, $Mn(NO_3)_2\cdot 4H_2O$ (0.062 g, 0.25 mmol) was dissolved in hot DMSO (10 mL) and added dropwise to a solution of $Na_2[Cu(L^x)_2]\cdot 4H_2O$ ($x=2$, 3; 0.25 mmol) dissolved in hot DMSO (10 mL) at 80°C. The resulting dark-green solution was filtered while hot and the filtrate was allowed to stand at RT. After several days, green polycrystalline solids of **2c** and **3c** appeared, which were filtered off and air-dried.

2c: Yield: 75%; IR (KBr): $\tilde{\nu}=3448$ (O−H), 2965 and 2918 (C−H), 1601 and 1626 (C=O) cm^{-1}; elemental analysis calcd (%) for $C_{28}MnCuH_{38}N_2O_8S_2$ (713): C 47.15, H 5.37, N 3.92, *S* 8.99; found: C 46.61, H 5.24, N 4.08, S 8.70.

3c: Yield: 75%; IR (KBr): $\tilde{\nu}=3448$ (O−H), 2963 and 2920 (C−H), 1602 and 1637 cm^{-1} (C=O); elemental analysis calcd (%) for $C_{33}MnCuH_{36}N_2O_{12}S_{2.5}$ (872): C 45.48, H 6.48, N 3.22, S 9.20; found: C 45.24, H 6.45, N 3.16, S 9.13.

$[CoCu(L^2)_2(DMSO)_2]\cdot DMSO\cdot 2H_2O$ (2d) and $[CoCu(L^3)_2(DMSO)_2]\cdot 0.5DMSO$ (3d): Compounds **2d** and **3d** were prepared by following the synthetic procedure reported previously for $[CoCu(L^1)_2(DMSO)_2]\cdot DMSO$ (**1d**).[11b] In a typical experiment, $Co(NO_3)_2\cdot 6H_2O$ (0.073 g, 0.25 mmol) was dissolved in hot DMSO (10 mL) and added dropwise to a solution of $Na_2[Cu(L^x)_2]\cdot 4H_2O$ ($x=2$ and 3; 0.25 mmol) dissolved in hot DMSO (10 mL) at 80°C. The resulting dark-green solution was filtered while hot and the filtrate was allowed to stand at RT. After several days, green polycrystalline solids of **2d** and **3d** appeared, and were filtered off and air-dried.

2d: Yield: 65%; IR (KBr): $\tilde{\nu}=3440$ (O−H), 2960 and 2945 (C−H), 1600 cm^{-1} (C=O); elemental analysis calcd (%) for $C_{30}H_{48}CoCuN_2O_{10}S_3$ (831): C 43.34, H 5.82, N 3.37, *S* 11.57; found: C 43.17, H 5.78, N 3.29, *S* 11.54.

3d: Yield: 70%; IR (KBr): $\tilde{\nu}=3432$ (O−H), 2960 and 2937 (C−H), 1603 and 1608 cm^{-1} (C=O); elemental analysis calcd (%) for $C_{32}H_{46}CoCuN_2O_8S_2$ (773): C 47.70, H 5.99, N 3.62, S 8.30; found: C 47.79, H 6.02 N 3.61, S 8.33.

Physical techniques: Elemental analyses (C, H, N and S) were carried out by the Microanalytical Service of the Universitat de València. ^1H NMR spectra were recorded at 250 MHz by using a Bruker AC 250 spectrometer. Chemical shifts are reported in parts per million (ppm) versus TMS with the residual proton signals of deuterated DMSO as the internal standard. IR spectra were recorded by using a Perkin–Elmer 882 spectrophotometer as KBr pellets. Variable-temperature dc and ac magnetic susceptibility measurements and variable-field magnetization measurements were carried out on powdered samples by using a Quantum Design SQUID magnetometer. The susceptibility data were corrected for the diamagnetism of the constituent atoms and the sample holder.

Crystal data collection and refinement: The X-ray diffraction data of **2a** and **3a** were collected at 100(2) K on crystals embedded in oil by using synchrotron radiation [$\lambda=0.7293$ (**2a**) and 0.7380 Å (**3a**)] at the BM16-CRG beamline in the ESRF (Grenoble, France). The quality of the data is far from optimal because of the poor diffraction of the crystals and partial loss of crystallinity during data collection. The brilliance of the synchrotron radiation allowed fast experiments to be carried out, and two satisfactory data sets were obtained that were carefully indexed, integrated and scaled by using the HKL2000 program.[22] All calculations for data reduction, structure solution and refinement were done by standard procedures (WINGX).[23] The structures of **2a** and **3a** were solved by direct methods and refined with full-matrix least-squares technique on F^2 by using the SHELXS-97 and SHELXL-97 programs.[24] Some disorder was found for the uncoordinated dimethylformamide molecule in **3a**, the atoms of which were refined anisotropically by applying some constraints with a fixed occupation factor of 0.5. The residual electron density was assigned to a not fully occupied position of the O(1w) atom from a water molecule of crystallization (the site occupancy factor was refined and once converged, it was fixed to that value for subsequent refinements). The hydrogen atoms of the organic ligands and dimethylformamide molecules were calculated and refined with isotropic thermal parameters, whereas those of the water molecule were neither found nor calculated. The final geometrical calculations and the graphical manipulations were carried out with PARST97 and CRYSTAL MAKER programs, respectively.[25] Unfortunately, no reliable information was obtained for complexes **1a**, **1b–3b** and **1c–3c** from the analysis of the powder diffraction patterns because of their quasi-amorphous nature.

CCDC 784413 (**2a**) and 784414 (**3a**) contain the supplementary crystallographic data for this paper. These data can be obtained free of charge from The Cambridge Crystallographic Data Centre via www.ccdc.cam.ac.uk/data_request/cif.

Acknowledgements

This work was supported by the MICINN (Spain; projects CTQ2007-61690, MAT2007-60660, CSD2007-00010 and CSD2006-00015), the Generalitat Valenciana (Spain; project PROMETEO/2009/108), the Gobierno Autónomo de Canarias (Spain; project PI2002/175) and the CNRS (France). E. P. and J.F.-S. acknowledge the MICINN and the Generalitat

Valenciana for a postdoctoral ("Juan de la Cierva") and a predoctoral grant, respectively.

[1] A. Caneschi, D. Gatteschi, N. Lalioti, C. Sangregorio, R. Sessoli, G. Venturi, A. Vindigni, A. Rettori, M. G. Pini, M. Novak, *Angew. Chem.* **2001**, *113*, 1810; *Angew. Chem. Int. Ed.* **2001**, *40*, 1760.
[2] R. J. Glauber, *J. Math. Phys.* **1963**, *4*, 294.
[3] D. Gatteschi, R. Sessoli, J. Villain, *Molecular Nanomagnets*, Oxford University Press, **2006**.
[4] a) R. E. P. Winpenny, *Adv. Inorg. Chem.* **2001**, *52*, 1; b) D. Gatteschi, R. Sessoli, *Angew. Chem.* **2003**, *115*, 278; *Angew. Chem. Int. Ed.* **2003**, *42*, 268; c) V. Marvaud, J. M. Herrera, T. Barilero, F. Tuyèras, R. Garde, A. Scuiller, C. Decroix, M. Cantuel, C. Desplanches, *Monatsh. Chem.* **2003**, *134*, 149; d) E. K. Brechin, *Chem. Commun.* **2005**, 5141; e) G. Aromí, E. K. Brechin, *Struct. Bonding (Berlin)* **2006**, *122*, 1; f) T. C. Stamatatos, G. Christou, *Inorg. Chem.* **2009**, *48*, 3308.
[5] a) C. Coulon, H. Miyasaka, R. Clérac, *Struct. Bonding (Berlin)* **2006**, *122*, 163; b) H. Miyasaka, M. Julve, M. Yamashita, R. Clérac, *Inorg. Chem.* **2009**, *48*, 3420; c) H. L. Sun, Z. M. Wanga, S. Gao, *Coord. Chem. Rev.* **2010**, *254*, 1081.
[6] a) A. Caneschi, D. Gatteschi, N. Lalioti, C. Sangregorio, R. Sessoli, G. Venturi, A. Vindigni, A. Rettori, M. G. Pini, M. Novak, *Europhys. Lett.* **2002**, *58*, 771; b) A. Caneschi, D. Gatteschi, N. Lalioti, R. Sessoli, L. Sorace, V. Tangoulis, A. Vindigni, *Chem. Eur. J.* **2002**, *8*, 286; c) L. Bogani, A. Caneschi, M. Fedi, D. Gatteschi, M. Massi, M. A. Novak, M. G. Pini, A. Rettori, R. Sessoli, A. Vindigni, *Phys. Rev. Lett.* **2004**, *92*, 207204; d) L. Bogani, C. Sangregorio, R. Sessoli, D. Gatteschi, *Angew. Chem.* **2005**, *117*, 5967; *Angew. Chem. Int. Ed.* **2005**, *44*, 5817; e) K. Bernot, L. Bogani, A. Caneschi, D. Gatteschi, R. Sessoli, *J. Am. Chem. Soc.* **2006**, *128*, 7947; f) N. Ishii, Y. Okamura, S. Chiba, T. Nogami, T. Ishida, *J. Am. Chem. Soc.* **2008**, *130*, 24.
[7] a) R. Clérac, H. Miyasaka, M. Yamashita, C. Coulon, *J. Am. Chem. Soc.* **2002**, *124*, 12837; b) H. Miyasaka, R. Clérac, K. Mizushima, K. Sugiura, M. Yamashita, W. Wernsdorfer, C. Coulon, *Inorg. Chem.* **2003**, *42*, 8203; c) A. Saitoh, H. Miyasaka, M. Yamashita, R. Clérac, *J. Mater. Chem.* **2007**, *17*, 2002; d) H. Miyasaka, A. Saitoh, M. Yamashita, R. Clérac, *Dalton Trans.* **2008**, 2422; e) M. Ferbinteanu, H. Miyasaka, W. Wernsdorfer, K. Sugiura, K. Nakata, M. Yamashita, C. Coulon, R. Clérac, *J. Am. Chem. Soc.* **2005**, *127*, 3090; f) H. Miyasaka, T. Madanbashi, K. Sugimoto, Y. Nakazawa, W. Wernsdorfer, K. Sugiura, M. Yamashita, C. Coulon, R. Clérac, *Chem. Eur. J.* **2006**, *12*, 7028.
[8] a) R. Lescouëzec, J. Vaissermann, C. Ruiz-Pérez, F. Lloret, R. Carrasco, M. Julve, M. Verdaguer, Y. Dromzée, D. Gatteschi, W. Wernsdorfer, *Angew. Chem.* **2003**, *115*, 1521; *Angew. Chem. Int. Ed.* **2003**, *42*, 1483; b) L. M. Toma, R. Lescouëzec, F. Lloret, M. Julve, J. Vaissermann, M. Verdaguer, *Chem. Commun.* **2003**, 1850; c) L. M. Toma, F. S. Delgado, C. Ruiz-Pérez, R. Carrasco, J. Cano, F. Lloret, M. Julve, *Dalton Trans.* **2004**, 2836; d) L. M. Toma, R. Lescouëzec, J. Pasán, C. Ruiz-Pérez, J. Vaissermann, J. Cano, R. Carrasco, W. Wernsdorfer, F. Lloret, M. Julve, *J. Am. Chem. Soc.* **2006**, *128*, 4842; e) L. M. Toma, R. Lescouëzec, S. Uriel, R. Llusar, C. Ruiz-Pérez, J. Vaissermann, F. Lloret, M. Julve, *Dalton Trans.* **2007**, 3690.
[9] a) T. Liu, D. Fu, S. Gao, Y. Zhang, H. Sun, G. Su, Y. Liu, *J. Am. Chem. Soc.* **2003**, *125*, 13976; b) S. Wang, J. L. Zuo, S. Gao, Y. Song, H. C. Zhou, Y. Z. Zhang, X. Z. You, *J. Am. Chem. Soc.* **2004**, *126*, 8900; c) H. R. Wen, C. F. Wang, Y. Song, J. L. Zuo, X. Z. You, *Inorg. Chem.* **2006**, *45*, 8942.
[10] a) E. Coronado, J. R. Galán-Mascarós, C. Martí-Gastaldo, *J. Am. Chem. Soc.* **2008**, *130*, 14987; b) E. Coronado, J. R. Galán-Mascarós, C. Martí-Gastaldo, *CrystEngComm* **2009**, *11*, 2143.
[11] a) E. Pardo, R. Ruiz-García, F. Lloret, J. Faus, M. Julve, Y. Journaux, F. S. Delgado, C. Ruiz-Pérez, *Adv. Mater.* **2004**, *16*, 1597; b) E. Pardo, R. Ruiz-García, F. Lloret, J. Faus, M. Julve, Y. Journaux, M. A. Novak, F. S. Delgado, C. Ruiz-Pérez, *Chem. Eur. J.* **2007**, *13*, 2054; c) E. Pardo, C. Train, R. Lescouëzec, Y. Journaux, J. Pasán, C. Ruiz-Pérez, F. S. Delgado, R. Ruiz-García, F. Lloret, C. Paulsen, *Chem. Commun.* **2010**, *46*, 2322.
[12] S. Zumer, *Phys. Rev. B* **1980**, *21*, 1298.
[13] a) H. Miyasaka, M. Yamashita, *Dalton Trans.* **2007**, 399; b) R. Sessoli, *Angew. Chem.* **2008**, *120*, 5590; *Angew. Chem. Int. Ed.* **2008**, *47*, 5508.
[14] a) W. Wernsdorfer, N. Aliaga-Alcalde, D. N. Hendrickson, G. Christou, *Nature* **2002**, *416*, 406; b) W. Wernsdorfer, S. Bhaduri, R. Tiron, D. N. Hendrickson, G. Christou, *Phys. Rev. Lett.* **2002**, *89*, 197201; c) K. Park, M. R. Pederson, S. L. Richardson, N. Aliaga-Alcalde, G. Christou, *Phys. Rev. B* **2003**, *68*, 020405; d) S. Hill, R. S. Edwards, N. Aliaga-Alcalde, G. Christou, *Science* **2003**, *302*, 1015.
[15] a) R. Tiron, W. Wernsdorfer, N. Aliaga-Alcalde, G. Christou, *Phys. Rev. B* **2003**, *68*, 140407(R); b) R. Tiron, W. Wernsdorfer, D. Foguet-Albiol, N. Aliaga-Alcalde, G. Christou, *Phys. Rev. Lett.* **2003**, *91*, 227203; c) C. Boskovic, R. Bircher, P. L. W. Tregenna-Piggott, H. U. Güdel, C. Paulsen, W. Wernsdorfer, A. L. Barra, E. Khatsko, A. Neels, H. Stoeckli-Evans, *J. Am. Chem. Soc.* **2003**, *125*, 14046.
[16] a) H. Miyasaka, K. Nakata, K. Sugiura, M. Yamashita, R. Clérac, *Angew. Chem.* **2004**, *116*, 725; *Angew. Chem. Int. Ed.* **2004**, *43*, 707; b) J. Yoo, W. Wernsdorfer, E. C. Yang, M. Nakano, A. L. Rheingold, D. N. Hendrickson, *Inorg. Chem.* **2005**, *44*, 3377; c) H. Miyasaka, K. Nakata, L. Lecren, C. Coulon, Y. Nakazawa, T. Fujisaki, K. Sugiur, M. Yamashita, R. Clérac, *J. Am. Chem. Soc.* **2006**, *128*, 3770.
[17] a) O. Kahn, Y. Pei, M. Verdaguer, J. P. Renard, J. Sletten, *J. Am. Chem. Soc.* **1988**, *110*, 782; b) H. O. Stumpf, Y. Pei, L. Ouahab, F. Leberre, E. Codjovi, O. Kahn, *Inorg. Chem.* **1993**, *32*, 5687; c) H. O. Stumpf, Y. Pei, O. Kahn, J. Sletten, J. P. Renard, *J. Am. Chem. Soc.* **1993**, *115*, 6738.
[18] a) P. J. Van Koningsbruggen, O. Kahn, K. Nakatani, Y. Pei, J. P. Renard, M. Drillon, P. Legoll, *Inorg. Chem.* **1990**, *29*, 3325; b) C. L. M. Pereira, A. C. Doriguetto, C. Konzen, L. C. B. Meira, N. G. Fernandes, Y. P. Mascarenhas, J. Ellena, M. Knobel, H. O. Stumpf, *Eur. J. Inorg. Chem.* **2005**, 5018; c) F. Lloret, M. Julve, J. Cano, R. Ruiz-García, and E. Pardo, *Inorg. Chim. Acta* **2008**, *361*, 3432.
[19] a) M. A. Girtu, C. M. Wynn, W. Fujita, K. Awaga, A. Epstein, *J. Phys. Rev. B* **1998**, *57*, R11058; b) J. A. Mydosh, *Spin Glasses: An Experimental Introduction*, Taylor & Francis, London, **1993**; c) D. Chowdhury, *Spin Glasses and Other Frustrated Systems*, Princeton University Press, New Jersey, **1986**; d) K. Moorjani, J. M. D. Coey, *Magnetic Glasses*, Elsevier, New York, **1984**; e) K. Binder, A. P. Young, *Rev. Mod. Phys.* **1986**, *58*, 801.
[20] a) K. S. Cole, R. H. Cole, *J. Chem. Phys.* **1941**, *9*, 341; b) C. J. F. Boettcher, *Theory of Electric Polarization*, Elsevier, Amsterdam, **1952**; c) S. M. Aubin, Z. Sun, L. Pardi, J. Krzysteck, K. Folting, L. J. Brunel, A. L. Rheingold, G. Christou, D. N. Hendrickson, *Inorg. Chem.* **1999**, *38*, 5329.
[21] a) J. D. Rinehart, K. R. Meihaus, J. R. Long, *J. Am. Chem. Soc.* **2010**, *132*, 7572; b) Y.-N. Guo, G.-F. Xu, P. Gamez, L. Zhao, S.-Y. Lin, R. Deng, J. Tang, H.-J. Zang, *J. Am. Chem. Soc.* **2010**, *132*, 8538.
[22] Z. Otwinowski, W. Minor in *Methods in Enzymology, Vol. 276, Macromolecular Crystallography, Part A* (Eds.: C. W. Carter, Jr., R. M. Sweet), **1997**, p. 307.
[23] L. J. Farrugia, *J. Appl. Crystallogr.* **1999**, *32*, 837.
[24] G. M. Sheldrick, SHELX-97, Programs for Crystal Structure Analysis release 97-2, Institut für Anorganische Chemie der Universität Göttingen, Göttingen, **1998**.
[25] a) M. Nardelli, *J. Appl. Crystallogr.* **1995**, *28*, 659; b) D. Palmer, *CRYSTAL MAKER* Cambridge University Technical Services, Cambridge, **1996**.

Received: July 23, 2010
Published online: January 24, 2011

